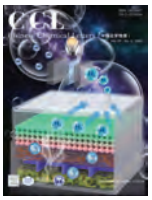
Chinese Chemical Letters 37 (2026) 111119

Contents lists available at ScienceDirect

Chinese Chemical Letters

journal homepage: www.elsevier.com/locate/cclet



Conjugated di-Cy5.5 derivative achieving strong light-harvesting ability beyond 808 nm for high-efficient antitumor photodynamic therapy

Hua Gu[a,b], Juan Zhang[a], Puan Yuan[b], Zhongyue Zheng[b], Wenkai Liu[b], Xiang Xia[a,b], Wen Sun[a,b], Jianjun Du[a,b,*], Jiangli Fan[a,b,*], Xiaojun Peng[b]

[a] Ningbo Institute of Dalian University of Technology, Ningbo 315016, China
[b] State Key Laboratory of Fine Chemicals, Frontier Science Center for Smart Materials, Dalian University of Technology, Dalian 116024, China

ARTICLE INFO

Article history:
Received 14 January 2025
Revised 17 March 2025
Accepted 19 March 2025
Available online 20 March 2025

Keywords:
Conjugated di-Cy5.5
NIR photosensitizer
Excited state regulation
Triplet-state quantum yields
Light harvesting
Photodynamic therapy

ABSTRACT

The performance of photosensitizers determines the effect of photodynamic therapy (PDT). At present, most photosensitizers are developed from fluorescent dyes, but it is difficult to possess both the good photophysical properties and photosensitive efficiency. In this work, an efficient strategy was developed to construct a cyanine-based near infrared (NIR) photosensitizer, **2LBCy5.5**, with an enlarged and twisted D-π-A-π-D structure by connecting two classical Cy5.5 dyes smartly with a dual-cationic benzo[1,2-*b*:4,5-*b*']dipyrrole group. The **2LBCy5.5** exhibited a maximum absorption at 802 nm with a great molar extinction coefficient of 4.2×10^5 L mol^{-1} cm^{-1}, compared with its parent Cy5.5 (692 nm with a molar extinction coefficient of 2.5×10^5 L mol^{-1} cm^{-1}). Furthermore, **2LBCy5.5** exhibited narrow energy gap of singlet-triplet ($\Delta E_{S\text{-}T}$) accelerated the intersystem crossing process (1.21 ns^{-1}) with a high triplet-excited-state quantum yield (26.1%) under 808 nm excitation, greatly contributing to reactive oxygen species (ROS) generation in type-I PDT. The excellent anti-tumor ability of **2LBCy5.5** was realized both under normoxic and hypoxic conditions. This study provides an effective and powerful approach for designing cyanine photosensitizers with strong capabilities in both photophysical properties (*e.g.*, NIR light-harvesting) and highly antitumor efficiency.

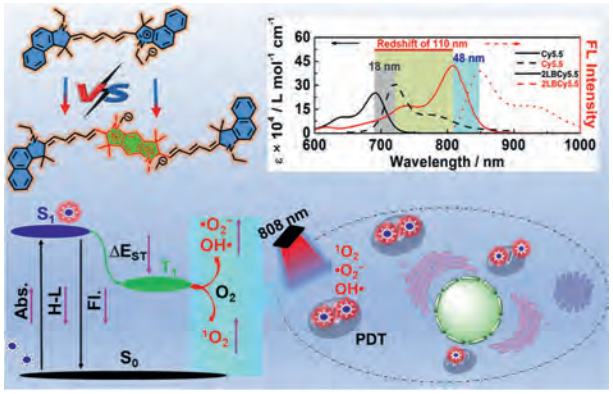
© 2026 Published by Elsevier B.V. on behalf of Chinese Chemical Society and Institute of Materia Medica, Chinese Academy of Medical Sciences.

Cyanine dyes possess outstanding photophysical properties, adjustable wavelength, biocompatibility, and biosafety, which have been widely applied in fields of chemistry, biology, and medicine [1,2]. For example, indocyanine green (ICG) is approved by the Food and Drug Administration (FDA) for optical imaging of vasculature and navigation surgery in clinic, with good tissue penetration capability (excited by 808 nm laser). Up to the present, therefore, various near infrared (NIR) photosensitizers have been developed based on pentamethine cyanine (Cy5) and heptamethine cyanine (Cy7) dyes for photodynamic therapy (PDT) of solid tumor [3–8]. As a kind of safe and noninvasive treatment, PDT exhibits charming characteristic for tumor therapy with good spatiotemporal controllability and without drug resistant [9–16]. For a good photosensitizer which is the key point of PDT, besides NIR light absorption, it should also have high efficiency of intersystem crossing (ISC) and long lifetime of excited states [4,5,11,15,16]. However, there are few efficient tactics to construct Cy7-based NIR photosensitizers, besides introducing heavy atoms (*e.g.*, I, Br, and Se) to enhance ISC process (S1→T1) [17–20]. Nevertheless, the heavy atom strategy usually produces $^1O_2$ as the only product which restricts the PDT effect heavily in hypoxic solid tumors, along with inevitable dark toxicity and the reduced lifetime of excited states [4,5,10]. Recently, the spin–orbit charge transfer intersystem crossing (SOCT-ISC) is introduced to improve the triplet yield [1,3,7,21–23]. For example, the anthracene-substituted Cy5 (at *meso*–position) is demonstrated to enrich the populations in high vibrational–rotational energy levels and subsequently improve $^1O_2$ generation [5]. However, the large twisted configuration always leads to heavy decline of extinction efficiencies of dyes along with an obvious blue-shift in absorption. Therefore, there are still significant challenges in how to develop an ingenious approach to transform a good NIR cyanine dye into an excellent cyanine photosensitizer while maintaining and even enhancing its photophysical properties.

The ISC efficiency and the NIR absorption of photosensitizers are directly related to $\Delta E_{S\text{-}T}$ (the band gap of singlet-excited and triplet-excited states) and $\Delta E_{H\text{-}L}$ (the band gap of lowest unoccupied molecular orbital (LUMO) and the highest occupied molecular orbital (HOMO)), respectively [24–27]. Actually, increasing conjugation of dyes is one of the most direct and effective methods

* Corresponding authors.
E-mail addresses: dujj@dlut.edu.cn (J. Du), fanjl@dlut.edu.cn (J. Fan).

https://doi.org/10.1016/j.cclet.2025.111119
1001-8417/© 2026 Published by Elsevier B.V. on behalf of Chinese Chemical Society and Institute of Materia Medica, Chinese Academy of Medical Sciences.



Scheme 1. Schematic illustration of cyanine structure, photophysical properties, ROS generation mechanism, and application in PDT.

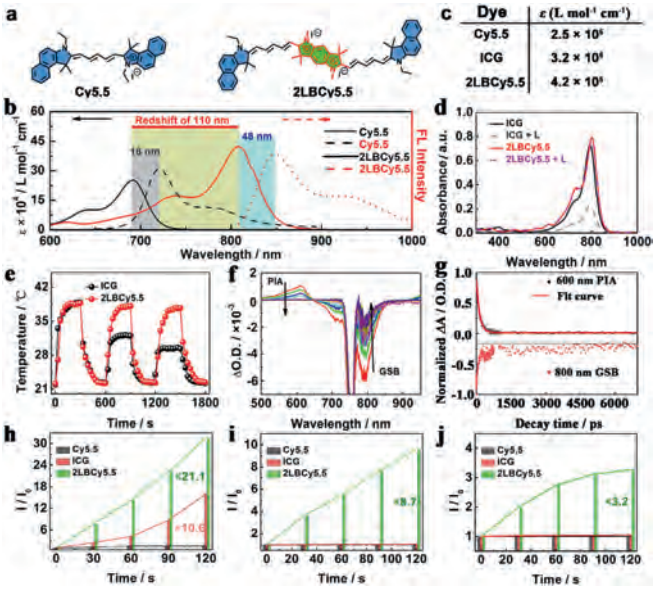


Fig. 1. (a) The structures of Cy5.5 (as control) and **2LBCy5.5**. (b) UV–vis-NIR spectra and fluorescence emission spectra of Cy5.5, ICG, and **2LBCy5.5** in DMSO, respectively. (c) The molar extinction coefficient of Cy5.5, ICG, and **2LBCy5.5** in DMSO, respectively. (d) Stability of **2LBCy5.5** and ICG against photobleaching. (e) Photothermal stability study of **2LBCy5.5** and ICG (20.0 μmol/L) during repeated heating and cooling cycles under 808 nm laser irradiation with 0.5 W/cm^2. (f) Femtosecond transient absorption spectra and (g) the kinetics of PIA and GSB of **2LBCy5.5**. The (h) $^1O_2$, (i) $^{\bullet}O_2^-$, and (j) $^{\bullet}OH$ measurement of Cy5.5, ICG, and **2LBCy5.5** upon laser irradiations (10 mW/cm^2) by using SOSG, DHE, and HPF as probes respectively, where I_0 and I are the fluorescence intensity at maximum emission peaks of ROS indicators in the presence of the photosensitive dyes before and after irradiation. ([**2LBCy5.5** and ICG] = 4 μmol/L and [SOSG, DHE, and HPF] = 10 μmol/L).

to benefit the extinction coefficient and adjust $\Delta E_{H\text{-}L}$. Moreover, $\Delta E_{S\text{-}T}$ also decreases along with $\Delta E_{H\text{-}L}$. Studies have shown that the introduction of D (electron donor)-π-A (electron acceptor) structure in dyes can change the decay property of the excited state, reduce the radiative transition (fluorescence performance), promote ISC, and prolong the triplet state lifetime effectively [28–31]. Therefore, compared with normal D-π-A structure, cyanine dyes with larger conjugation system (such as D-π-A-π-D structure) could much more effectively red-shift absorption/emission, increase intramolecular electron transfer, and reduce $\Delta E_{S\text{-}T}$. Most importantly, the linear extension of cyanine dyes could lead to the proper twisted structure, increasing the charge separation that make electron transfer possible with O_2, H_2O, and other surrounding molecules (Scheme 1) [2,24,24,32–34].

Herein, as a-proof-of-concept, a novel D-π-A-π-D type of di-Cy5.5 derivative (**2LBCy5.5**) was constructed based on a classical fluorescent dye Cy5.5, with dual-cationic benzo[1,2-*b*:4,5-*b*′]dipyrrole (as an electron acceptor) bridging two Cy5.5 molecules (as electron donors). The **2LBCy5.5** exhibits a maximum absorption wavelength of 802 nm, with a redshift of 110 nm compared with Cy5.5 and much greater molar extinction coefficient of 4.2×10^5 L mol^{-1} cm^{-1} than that of Cy5.5 (692 nm with molar extinction coefficient of 2.5×10^5 L mol^{-1} cm^{-1}) and ICG (795 nm with molar extinction coefficient of 3.2×10^5 L mol^{-1} cm^{-1}). Furthermore, **2LBCy5.5** showed low $\Delta E_{H\text{-}L}$ and $\Delta E_{S\text{-}T}$, fast ISC rate, and high triplet-excited state yield, compared to its parent Cy5.5. The **2LBCy5.5** showed a good anti-tumor ability under both normoxic and hypoxic conditions by producing various reactive oxygen species (ROS) under 808 nm light irradiation. This work provides a new approach for designing high-performance NIR photosensitizers with improved light-harvesting ability, photosensitizing efficiency, and stability.

2LBCy5.5 (Fig. 1a) was synthesized with the dual-cationic benzo[1,2-b:4,5-b′]dipyrrole as an acceptor coupled two Cy5.5 molecules, according to the routes provided in Fig. S1 (Supporting information), which was confirmed by ^{1}H nuclear magnetic resonance (NMR), ^{13}C NMR, and high resolution mass spectrometer (HRMS) (Figs. S2–S12 in Supporting information) [35–37].

The photophysical properties of dyes were investigated, such as ultraviolet-visible (UV–vis)-NIR absorption and fluorescence emission. As shown in Fig. 1b, **2LBCy5.5** exhibited a maximum absorption at 802 nm in dimethylsulfoxide (DMSO), which redshifted about 110 nm compared to Cy5.5 (692 nm) and even exceeded that of ICG (795 nm). The maximum fluorescence emission of Cy5.5, ICG, and **2LBCy5.5** located at 720, 833, and 850 nm in DMSO, with Stokes shifts of 28, 37, and 48 nm, respectively. Meanwhile, the molar extinction coefficient of **2LBCy5.5** reached 4.2×10^5 L mol^{-1} cm^{-1}, which was much more than that of Cy5.5 (2.5×10^5 L mol^{-1} cm^{-1}) and ICG (3.2×10^5 L mol^{-1} cm^{-1}), suggesting its excellent light-harvesting capability (Fig. 1c and Fig. S13 in Supporting information). The fluorescence quantum yield of **2LBCy5.5** was 0.06, which was lower than that of Cy5.5 (0.33).

Generally, the stability of cyanine dyes is the basis for their functions. Upon 808 nm laser irradiation (10 W/cm^2, 10 min), the absorbance of ICG decreased about 62%, whereas there was little change for **2LBCy5.5**, demonstrating good stability against photobleaching (Fig. 1d). Furthermore, the stability of **2LBCy5.5** was evaluated by high-power irradiation (0.5 W/cm^2) for three heating and cooling cycles. As shown in Fig. 1e, **2LBCy5.5** exhibited a repeatable temperature variation without absorption changes with acceptable photothermal conversion efficiency of 22.3% (Fig. S14 in Supporting information). However, under the same conditions, the maximum temperature of ICG decreased obviously after three cycles. These results indicated excellent photostability of **2LBCy5.5**.

In addtion, femtosecond transient absorption spectra were obtained to analyze the excited-state energy dissipation pathways (Fig. 1f). The positive and negative signals signify the S_1 to S_n transition (photoinduced absorption (PIA)) and S_0 to S_1 transition (ground-state bleaching (GSB)), respectively [38,39]. Since the excited-state energy dissipation pathways are mainly composed of radiative transition (k_r represents the radiative decay rate), nonradiative transition (k_{nr} represents the nonradiative decay rate) and ISC process (k_{ISC} represents the ISC decay rate) [7,29,40–42]. According to the GSB remaining/GSB initial ratio and defined as $k_x/(k_{ISC} + k_{nr} + k_r)$ (x stands for ISC, nr or r). Thus, by fitting the decay kinetics (Fig. 1g), the total decay rate ($k_{ISC} + k_{nr} + k_r$) was obtained, 2.89 ns^{-1}. Subsequently, the k_r value was 0.25 ns^{-1} (9.6% proportion), the k_{nr} value was 1.43 ns^{-1} (49.4% proportion) and the

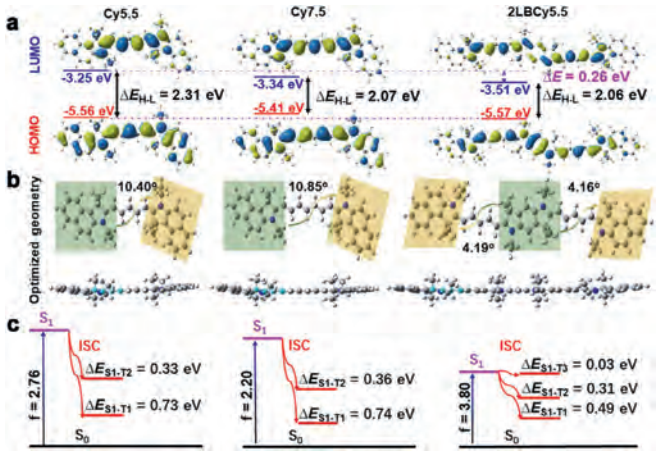


Fig. 2. Molecular orbital amplitude plots of Cy5.5, Cy7.5, and **2LBCy5.5**, calculated using the Gaussian 16 B3LYP/def2svp program. (a) Calculated HOMO and LUMO geometries, (b) optimized molecular structure, and (c) oscillator strength (*f*), singlet energy level (S_1), triplet energy level (T_1), and $\Delta E_{S\text{-}T}$ values.

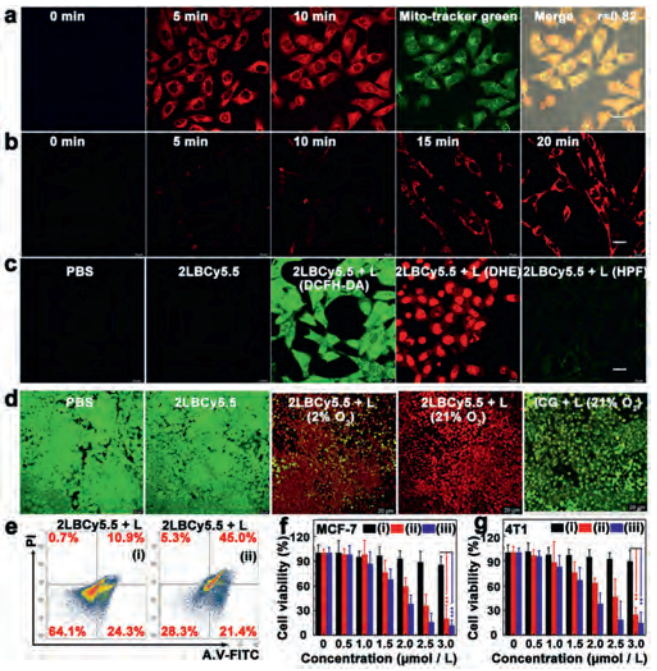


Fig. 3. Confocal images of cellular uptake and colocalization of **2LBCy5.5** (2 μmol/L) in MCF-7 (a) and MCF-10A cells (b) at different times, and (c) the ROS detected of **2LBCy5.5** (2 μmol/L) in MCF-7 cells under 808 nm laser irradiation with SOSG, DHE, and HPF as detection probes for $^1O_2$, $^{\bullet}O_2^-$, and $^{\bullet}OH$, respectively. *In vitro* PDT of **2LBCy5.5**. Confocal images of (d) calcein-AM (green)/PI (red) in MCF-7 cells treated under different experimental conditions. (e) Flow cytometry analysis of MCF-7 cells (i was hypoxic conditions, ii was normoxic conditions) and (f, g) cell viability of MCF-7 and 4T1 cells incubated with different concentrations of **2LBCy5.5** (results are presented as mean ± SD, $n = 5$). Where, i, ii, and iii are represented the **2LBCy5.5** without laser irradiation, **2LBCy5.5** with laser irradiation under hypoxia condition and **2LBCy5.5** with laser irradiation under normoxia condition ([**2LBCy5.5** or ICG] = 2 μmol/L, 808 nm laser irradiation with 30 mW/cm^2, 10 min). *P*-values were calculated using Student's *t*-test. $^{**}P < 0.01$, $^{***}P < 0.001$. Scale bar: 20 μm.

k_{ISC} value was 1.21 ns^{-1} (41.0 % proportion), which indicated that the balance of excited state decay was more in favor of ISC process for PDT. As a result, the triplet state yield of **2LBCy5.5** was determined to be 26.1 %, higher than that of Cy7 derivative (17 %–22 %) under the same conditions [7,29], implying a greater T1 population and a stronger ROS-generating capacity.

Thus, under 808 nm laser irradiation with 10 W/cm^2 power, the ROS generation ability of $^1O_2$, $^{\bullet}O_2^-$, and $^{\bullet}OH$ of Cy5.5, ICG and **2LBCy5.5** were measured using singlet oxygen sensor green probe (SOSG), dihydroethidium (DHE), and hydroxyphenyl fluorescein (HPF) as indicators, respectively. As shown in Figs. 1h–j and Figs. S15–S17 (Supporting information), the characteristic fluorescence signals of SOSG (525 nm), DHE (610 nm), and HPF (515 nm) showed no fluorescence changes in the presence of ICG or Cy5.5, while gradually enhanced in the presence of **2LBCy5.5** upon laser irradiation, indicating both type-I and type-II ROS-generating mechanisms for **2LBCy5.5**. More importantly, **2LBCy5.5** showed higher ROS generation yield (about 10.6-/21.1-fold of $^1O_2$, ~8.7-fold of $^{\bullet}O_2^-$, and 3.2-fold of $^{\bullet}OH$) than that of ICG or Cy5.5 (as references), respectively. Therefore, **2LBCy5.5** can be used for both normoxia and hypoxia PDT.

To further interpret the photosensitization mechanism of **2LBCy5.5**, the density functional theory (DFT) of Cy5.5, Cy7.5 and **2LBCy5.5** was executed. The LUMO and HOMO energy levels of Cy5.5 were −3.25 and −5.56 eV with $\Delta E_{H\text{-}L}$ of 2.31 eV (Fig. 2a). As the conjugate structure was extended, the LUMO, HOMO, and $\Delta E_{H\text{-}L}$ of Cy7.5 were all changed to −3.34, −5.41, and 2.07 eV, respectively. However, **2LBCy5.5** exhibited strong electron-withdrawing ability, resulting in a low LUMO value of −3.51 eV. And $\Delta E_{H\text{-}L}$ of **2LBCy5.5** was 2.06 eV, lower than that of Cy7.5, which matched well with its red-shifted absorption. In addition, the electron-hole diagram of excited states calculated by time dependent (TD)-DFT also proved that **2LBCy5.5** has higher electron delocalization and charge separation states than those of Cy5.5 and Cy7.5 due to the dual-cation fused indole-induced intramolecular charge transfer (ICT) effect, which was conducive to electron hole transport and promoted excited state electron transfer to generate type-I ROS [8,25,29]. Furthermore, the optimized molecular conformations of Cy5.5, Cy7.5, and **2LBCy5.5** were investigated (Fig. 2b). The dihedral angles of the two terminal indole groups in Cy5.5 and Cy7.5 were 10.40° and 10.85°, respectively. In contrast, the dihedral angle between the terminal indole group and the fused indole group in the **2LBCy5.5** was only 4.16° (or 4.19°), indicating good planar structure. Even the distant terminal indole group in **2LBCy5.5** had a dihedral angle of only 8.35°, which might be the main factor leading to the increase in the molar extinction coefficient of **2LBCy5.5**. Additionally, the oscillator strength (*f*) and the $\Delta E_{S\text{-}T}$ values between the lowest singlet (S_1) and triplet energy levels (T_1) of the photosensitive dyes were also calculated in detail (Fig. 2c). Oscillator strength is an important physical parameter to characterize the absorption or emission of atoms, which is positively correlated to the absorption peak area and the molar extinction coefficient [7,40,43–45]. According to DFT, the *f* values of Cy5.5, Cy7.5, and **2LBCy5.5** were 2.76, 2.20, and 3.80, respectively, which fit the trend of molar extinction coefficients. The $\Delta E_{S1\text{-}T1}$ (0.49 eV) of **2LBCy5.5** was apparently decreased compared with that of Cy7.5 (0.74 eV) and Cy5.5 (0.73 eV). What is more, the $\Delta E_{S1\text{-}T3}$ of **2LBCy5.5** was 0.03 eV, much lower than the values of $\Delta E_{S1\text{-}T1}$ and $\Delta E_{S1\text{-}T2}$, indicating a potential ISC process from the S_1 state to the T_3 state. These theoretical results are consistent with experimental results.

Considering the excellent ROS generation ability, *in vivo* PDT of **2LBCy5.5** was studied. As shown in Fig. 3a, **2LBCy5.5** was rapidly taken up by MCF-7 cells within 10 min. The fluorescence signals of **2LBCy5.5** were overlapped with those of the Mito-green tracker, indicating an excellent mitochondrial-targeting function (Pearson's correlation coefficient is 0.82). However, a weak fluorescence signal was observed in MCF-10A cells under the same incubation period, and it required 20 min to achieve maximum brightness (*i.e.*, optimal enrichment), which is twice the duration observed in tumor cells (Fig. 3b). The above difference indicated that **2LBCy5.5** could discriminate normal cells from cancer cells to

some extent, potentially attributed to its dual cationic structure, which contributes to its preferential targeting of tumor cells with higher electronegativity [29,45–49]. Furthermore, we investigated the ROS generation performance in MCF-7 cells. Commercially available reagents SOSG, DHE, and HPF were used as detection probes for $^1O_2$, $^{\bullet}O_2^-$, and $^{\bullet}OH$, respectively. As shown in Fig. 3c, the significant fluorescent signals of SOSG, DHE, and HPF, were observed under 808 nm laser irradiation, indicating intracellular generation of $^1O_2$, $^{\bullet}O_2^-$, and $^{\bullet}OH$, which contributed to anti-tumor PDT under both hypoxic and normoxic environment.

To further verify the antitumor ability of **2LBCy5.5**, calcein-AM (green fluorescence for live cells) and propidium iodide (PI, red fluorescence for dead cells) were used for staining experiments. In Fig. 3d and Fig. S18 (Supporting information), a strong green fluorescence signal was observed in the control group treated with phosphate buffer saline (PBS) alone or **2LBCy5.5** (or ICG) alone, indicating their good biocompatibility. ICG cannot kill MCF-7 cells (green fluorescence under laser irradiation) under both normoxia and hypoxic conditions. In contrast, MCF-7 cells treated with **2LBCy5.5** and 808 nm laser irradiation were killed efficiently (bright red fluorescence) under both normoxic and hypoxic conditions. Since **2LBCy5.5** was localized in mitochondria of cells, commercially available JC-1 was employed as a probe to test the integrity of the mitochondrial membrane. As shown in Fig. S19 (Supporting information), under normoxia or hypoxia, JC-1 existed as a monomer in cells (green fluorescence) for the **2LBCy5.5** + L group, which was consistent with the result of the positive control group (CCCP), indicating that **2LBCy5.5**-mediated PDT significantly depolarized mitochondria. Next, flow cytometry was employed to assess the mechanism of photoinduced cytotoxicity. As shown in Fig. 3e and Fig. S20 (Supporting information), the MCF-7 cells underwent apoptosis with the pyroptosis index of 66.3 % after treatment with **2LBCy5.5** and 808 nm laser irradiation. Lastly, the *in vitro* tumor PDT effect of **2LBCy5.5** was evaluated by the MTT assay (Figs. 3f and g), and **2LBCy5.5** was found to have negligible toxicity to MCF-7 and 4T1 cells in the absence of laser irradiation, with cell survival up to 95 %. However, under laser irradiation, **2LBCy5.5** exhibited superior PDT performance with increasing concentrations in both normoxia and hypoxia condition.

The excellent tumor-targeting properties and PDT performance of **2LBCy5.5** motivated us to explore its anti-tumor effects *in vivo*. All *in vivo* studies were approved by the Dalian Medical University Animal Care and Use Committee (approval number: DUTNI230309-01). A tumor-bearing BALB/c mouse model was established with subcutaneous inoculation of 4T1 cells on the upper side of the right lower limb. When the tumor volume reached about 100 mm^3, all tumor-bearing BALB/c mice were randomly divided into four groups for *in vivo* anti-cancer PDT. Before treatment, fluorescence imaging was executed to record after the injection of **2LBCy5.5** through the caudal vein to obtain the optimal time point for PDT. As shown in Fig. 4a, with the extension of time, the fluorescence signal at the tumor site gradually increased and reached the maximum at 3 h, wherein **2LBCy5.5** was mainly enriched in the tumor site, followed by the liver and kidney. Therefore, the best treatment time was 3 h after tail vein injection.

Based on the above results, *in vivo* PDT was conducted after 2.5 h tail vein injection of **2LBCy5.5** by using 808 nm laser irradiation (100 mW/cm^2) for 10 min. After the laser irradiation, the changes in body weight and tumor volume of all the mice were continuously monitored for 15 d to estimate the PDT effect. As illustrated in Fig. 4c, all the mice grew well and exhibited no obvious difference during the treatment, indicating low side effects of **2LBCy5.5**. And the tumors in blank group (treated with PBS) and the control group (treated with **2LBCy5.5**) increased gradually about 10 times compared to their original volumes (Figs. 4b and d). As a sharp contrast, the tumors treated with **2LBCy5.5** + L (808 nm laser) underwent necrosis and eventually disappeared entirely, which demonstrated the high PDT efficiency of **2LBCy5.5**. Hematoxylin and eosin (H&E) staining revealed significant morphological damage to tumor tissue following photosensitizer-mediated PDT, with no observed cell necrosis or inflammation in major organs (such as the heart, liver, spleen, lung, and kidney) (Fig. 4e and Fig. S21 in Supporting information). Simultaneously, there were no abnormal liver and kidney function indexes before and after treatment (Fig. 4f (i)–(iii)), which showed that **2LBCy5.5** has no negative effect on the functions of the liver and kidney. These findings suggested that **2LBCy5.5** exhibited good anti-tumor effects and biocompatibility.

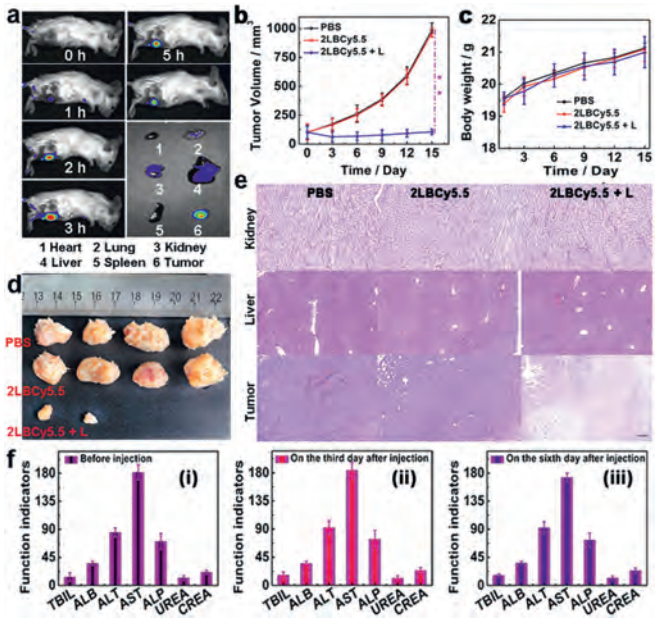


Fig. 4. *In vivo* PDT of **2LBCy5.5**. (a) The real-time fluorescence imaging of tumor-bearing mice and major organs after injection of **2LBCy5.5**. The tumor volume (b) and body weights (c) of the mice after different treatments. (d) Images of tumors harvested in mice from different groups at 15 days of post-treatment. (e) HE staining of tumor sections from different treatment groups after 15 days of treatment. (f) Hematological assessment of liver and kidney function indicators of mice at different post-injection times. Where, i, ii and iii are represented the different time of before injection, on the third day after injection and on the sixth day after injection, respectively). Scale bar: 100 μm. Data were expressed as mean ± SD ($n = 4$). $^{**}P < 0.01$ determined by Student's *t*-test.

In summary, the conjugated di-Cy5.5 derivative, **2LBCy5.5**, was successfully developed by conjugating two classical fluorescent dyes Cy5.5 with dual-cationic benzo[1,2-*b*:4,5-*b*′]dipyrrole group. As a result, **2LBCy5.5** showed a significant red shift in absorption/emission wavelength (802 and 850 nm, respectively), especially with a significantly enhanced molar extinction coefficient as high as 4.2×10^5 L mol^{-1} cm^{-1}. Because the extend conjugation results in strong ICT effect that endowed **2LBCy5.5** with a narrow $\Delta E_{H\text{-}L}$ and $\Delta E_{S\text{-}T}$, which promoted ISC progress efficiently and following excellent type-I and type-II ROS-generation capacity. Therefore, **2LBCy5.5** showed good anti-tumor ability under both normoxic and hypoxic conditions. In short, a simple and effective strategy was developed for constructing high-performance photosensitive dyes with excellent NIR light-harvesting ability, photosensitive ability, and photostability.

Declaration of competing interest

The authors declare that they have no known competing financial interests or personal relationships that could have appeared to influence the work reported in this paper.

CRediT authorship contribution statement

Hua Gu: Writing – original draft, Validation, Software, Resources, Project administration, Investigation, Funding acquisition, Formal analysis, Data curation, Conceptualization. **Juan Zhang:** Visualization, Validation, Methodology, Formal analysis. **Puan Yuan:** Software, Methodology, Data curation. **Zhongyue Zheng:** Validation, Software. **Wenkai Liu:** Software. **Xiang Xia:** Software, Data curation. **Wen Sun:** Funding acquisition. **Jianjun Du:** Writing – review & editing, Funding acquisition, Conceptualization. **Jiangli Fan:** Writing – review & editing, Funding acquisition, Conceptualization. **Xiaojun Peng:** Writing – review & editing, Conceptualization.

Acknowledgments

This work was financially supported by the National Natural Science Foundation of China (Nos. 21925802, 22308049, 22338005), Liaoning Provincial Science and Technology Joint Fund (Nos. 2023JH2/101800039, 2023JH2/101800037), Liaoning Binhai Laboratory (No. LBLB-2023-03), the Fundamental Research Funds for the Central Universities (No. DUT22LAB601), the China Postdoctoral Science Foundation (No. 2023M740486).

Supplementary materials

Supplementary material associated with this article can be found, in the online version, at doi:10.1016/j.cclet.2025.111119.

References

[1] A. Sharma, P. Verwilst, M. Li, et al., Chem. Rev. 124 (2024) 2699–2804.
[2] J. Yuan, H. Yang, W. Huang, et al., Chem. Soc. Rev. 54 (2025) 341–366.
[3] X. Zhao, J. Du, W. Sun, et al., Acc. Chem. Res. 57 (2024) 2582–2593.
[4] X. Yuan, J. Zhou, L. Yuan, et al., Sci. China Chem. 68 (2025) 826–865.
[5] X. Zhao, S. Long, M. Li, et al., J. Am. Chem. Soc. 142 (2020) 1510–1517.
[6] X. Zhao, Q. Yao, S. Long, et al., J. Am. Chem. Soc. 143 (2021) 12345–12354.
[7] X. Zhou, C. Shi, S. Long, et al., ACS Cent. Sci. 9 (2023) 1679–1691.
[8] F. Han, S. Abedi, S. He, et al., Adv. Sci. 11 (2024) 2305761.
[9] T. Pham, V. Nguyen, Y. Choi, et al., Chem. Rev. 121 (2021) 13454–13619.
[10] W. Fan, P. Huang, X. Chen, Chem. Soc. Rev. 45 (2016) 6488–6519.
[11] W. Su, X. Luo, P. Li, et al., Chin. Chem. Lett. 35 (2024) 109522.
[12] K. Teng, D. Zhang, B. Liu, et al., Angew. Chem. Int. Ed. 63 (2024) e202318783.
[13] X. Liu, J. Li, F. Zhang, et al., Sci. China Chem. 67 (2024) 2314–2324.
[14] Y. Yang, J. Zhang, Y. Wang, et al., Chin. Chem. Lett. 36 (2025) 110834.
[15] Z. Cui, D. Zhang, Y. Huang, et al., Chin. Chem. Lett. 36 (2025) 110460.
[16] S. Zhen, Z. Xu, M. Suo, et al., Adv. Mater. 37 (2025) 2411133.
[17] N. Sellet, J. Frey, M. Cormier, et al., Chem. Sci. 15 (2024) 8639–8650.
[18] J. Yu, Y. Wen, M. Li, Adv. Funct. Mater. 34 (2024) 2402663.
[19] Y. Yue, B. Li, D. Wang, et al., Adv. Funct. Mater. 35 (2024) 2414542.
[20] H. Wen, Q. Wu, X. Xiang, et al., ACS Appl. Mater. Interfaces 16 (2024) 61739–61750.
[21] D. Liu, A. El-Zohry, M. Taddei, et al., Angew. Chem. Int. Ed. 59 (2020) 11591–11599.
[22] Zhao X, S. He, W. Chi, et al., Adv. Sci. 9 (2022) 2202885.
[23] M. Williams, I. Schlesinger, R. Jacobberger, et al., J. Am. Chem. Soc. 144 (2022) 18607–18618.
[24] H. Huang, Q. Liu, J. Zhu, et al., Aggregate 6 (2025) e706.
[25] W. Liu, S. He, X. Ma, et al., Angew. Chem. Int. Ed. 63 (2024) e202484761.
[26] H. Janeková, S. Fisher, T. Šolomek, et al., Chem. Sci. 16 (2025) 1677–1683.
[27] C. You, Y. Zhu, J. Zhu, et al., Angew. Chem. Int. Ed. 64 (2024) e202417865.
[28] V. Nguyen, Z. Zhao, B. Tang, et al., Chem. Soc. Rev. 51 (2022) 3324–3340.
[29] H. Gu, W. Liu, W. Sun, et al., Chem. Sci. 13 (2022) 9719–9726.
[30] Y. Tang, H. Bisoyi, X. Chen, et al., Adv. Mater. 35 (2023) 2300232.
[31] H. Gu, W. Liu, H. Li, et al., Coord. Chem. Rev. 473 (2022) 214803.
[32] G. Gopika, P. Hari Prasad, A. Lekshmi, et al., Mater. Today Proc. 46 (2021) 3102–3108.
[33] X. Ma, Y. Huang, S. Abedi, et al., CCS Chem. 4 (2022) 1961–1976.
[34] Y. Yue, J. Ai, W. Chi, et al., Adv. Mater. 36 (2024) 2408450.
[35] H. Shindy, Dyes Pigm. 145 (2017) 505–513.
[36] O. Klochko, I. Fedyunyayeva, S. Khabuseva, et al., Dyes Pigm. 85 (2010) 7–15.
[37] F. Mihailenko, A. Boguslavskaya, A. Kiprianov, Chem. Heter. Comp. 7 (1971) 578–580.
[38] C. Ruckebusch, M. Sliwa, P. Pernot, et al., J. Photoch. Photobio. C: Photoch. Rev. 13 (2012) 1–27.
[39] R. Sension, T. McClain, R. Lamb, et al., J. Am. Chem. Soc. 145 (2023) 14070–14086.
[40] X. Xia, C. Shi, S. He, et al., Adv. Funct. Mater. 33 (2023) 2300340.
[41] B. Dereka, A. Rosspeintner, Z. Li, et al., J. Am. Chem. Soc. 138 (2016) 4643–4649.
[42] J. Kim, R. Kishi, E. Kayahara, et al., Angew. Chem. Int. Ed. 59 (2020) 16989–16996.
[43] M. Yang, X. Ou, J. Zhang, et al., Adv. Funct. Mater. 35 (2024) 2411838.
[44] Y. Li, J. Zhang, S. Liu, et al., Adv. Funct. Mater. 31 (2021) 2102213.
[45] M. Li, T. Xiong, J. Du, et al., J. Am. Chem. Soc. 141 (2019) 2695–2702.
[46] M. Wu, M. Gu, J. Leung, et al., Small 17 (2021) 2101770.
[47] M. Li, S. Long, Y. Kang, et al., J. Am. Chem. Soc. 140 (2018) 15820–15826.
[48] G. Li, Y. Huang, Q. Feng, et al., Molecules 19 (2014) 12224–12241.
[49] R. Horobin, J. Stocker, F. Rashid-Doubell, Histochem. Cell Biol. 139 (2013) 623–637.